JMEPEG (2010) 19:976–983
DOI: 10.1007/s11665-009-9566-8

1059-9495/$19.00

Structure and Property Studies on Austempered and As-Cast Ausferritic Gray Cast Irons

Aravind Vadiraj, G. Balachandran, and M. Kamaraj

(Submitted April 27, 2009; in revised form August 17, 2009)

A high-strength and wear-resistant alloyed gray iron with ausferritic microstructure on solidification directly from molten condition could be made in a Ni and Mo alloyed gray cast iron. The as-cast ausferritic cast iron was compared with two conventionally austempered gray iron with and without Ni and Mo additions. The various phase constitution and volume fractions were analyzed using optical, SEM and XRD analyses. The various aspects of the alloy chemistry and processing conditions have been correlated with the microstructure and mechanical properties obtained. The analysis showed that the Ni-Mo alloyed austempered gray iron and the directly as-cast austempered gray iron had similar phase constitutions. The strength of the direct as-cast alloy with ausferritic microstructure was higher than the others due to its higher austenite content and carbide distribution. The wear rate of the conventionally austempered Ni and Mo containing alloy and direct as-cast ausferritic alloys is 20% of the austempered gray iron without Ni and Mo with friction coefficient less than 0.4.

Keywords ausferrite, austempering, cast iron

1. Introduction

Conventional gray cast iron with flake graphite networks along with dense pearlite matrix is preferred for applications such as brake plate and clutch pressure plate in automobiles. The austempering heat treatment is usually carried out on gray irons to obtain a more wear-resistant microstructure with acicular ferrite in a stable ausferritic matrix. The austempering heat treatment involves austenitizing in the range of 850-920 °C, followed by salt bath heat treatment in the range of 280-500 °C. It is also possible to develop ausferrite microstructure directly from the as-cast condition with suitable alloying addition and cooling rate. Alloying additions to gray iron significantly alter the phase transformation sequence to generate a range of microstructures. Alloying additions such as Mn, Cu and Mo to gray iron have been reported to produce ausferritic structures directly in cast condition (Ref 1, 2). Wide range of microstructures such as austenite, pearlite, ausferrite and martensite can be obtained in as-cast alloys by systematically varying the alloying additions such as Mo, Mn, Si and Cu. At low Mo levels, the phase transformations in a hypoeutectic cast iron follow the sequence (Ref 1, 2):

$$L \rightarrow \gamma + L \rightarrow \gamma + G_f \text{ (eutectic)} \rightarrow \alpha + P \text{ (eutectoid)} + G_f$$

Higher amounts of alloying additions are reported to shift the C-curve to the right side delaying the diffusion transformation product region to longer times. This alters the bainite region appreciably, thereby allowing the formation of direct ausferrite structure as per the following sequence:

$$L \rightarrow \gamma + L \rightarrow \gamma + G_f \rightarrow \gamma + \alpha_B \text{ (ausferrite)} + G_f$$

The typical alloying modification carried out to get direct ausferritic microstructure in the as-cast condition is shown in Table 1. The concentration and type of alloying additions affect the type of acicular ferrite that forms within the austenite phase during continuous cooling. Alloy 1 has 3.2% C content, Mn (0.68-2.34%) and Si (1.41-2.32%) with 0.32% Mo promote ausferritic structure.

The alloying elements shift the pearlite transformation regime in the CCT diagram to the right while the bainitic transformation regime is retained. For low Mo levels ($<1.0\%$) at 0.55%Mn-1%Cu, the matrix microstructure consisted of carbide-free bainitic ferrite and carbon-enriched residual austenite. Large concentrations of alloying element Mn (1-1.5%) in cast iron with 1%Cu-0.32%Mo increase the hardenability of the alloy to such an extent that some martensite (1-5%) is generated during continuous cooling. The microstructure may also have some carbide formation associated with segregation to eutectic cell boundaries. In the alloy with 0.55% Mn alloy, when Mo content $>0.53\%$ generates ausferritic structure with increasing Cu content.

In automotive applications, austempered gray iron can be used for applications such as engine cylinder liner, piston ring, brakes, clutch, etc., where the ausferrite phase provide higher wear resistance at almost the same thermal conductivity of pearlitic gray iron (Ref 3, 4). The ausferritic phase hardens during mechanical deformation at the rubbing interface due to strain-induced martensite formation (Ref 5). The ausferritic structures have higher capacity to resist thermal distortion compared to pearlitic cast irons (Ref 6). Although the gray irons are brittle due to flake graphite, the austenite phase can give improved toughness in comparison to softer pearlitic gray irons (Ref 7).

Aravind Vadiraj and **G. Balachandran**, Advanced Engineering, Ashok Leyland Technical Center, Vellivoyalchavadi, Chennai 600103, India; and **M. Kamaraj**, Department of Metallurgical and Materials Engineering, Indian Institute of Technology Madras, Chennai 600036, India. Contact e-mail: aravindmail@yahoo.com.

Table 1 Composition and microstructure of cast irons in literature and their influence on mechanical properties (Ref 1, 2)

Alloy chemistry, wt.%	Microstructure
Fe-3.2C-1.0Cu-Mn varied up to 2.75	Pearlite with low fraction of martensite
Fe-3.2C-1.0Cu-Si varied up to 2.95	Pearlite with low fraction of martensite
Fe-3.2C-1.0Cu-0.55Mn-2.0Si-(0.11-0.22)Mo	100% pearlite
Fe-3.2C-1.0Cu-0.55Mn-2.0Si-(0.31-0.73)Mo	(0.8-28.7)% austenite + (4.7-69)% ausferrite + (94.5-2.3)% pearlite
Fe-3.2C-1.0Cu-0.55Mn-2.0Si-(0.95-1.17)Mo	(31.9-31.3)% austenite + (68.1-68.7)% ausferrite
Fe-3.2C-1.0Cu-0.32Mo-0.68 to 0.88Mn-(1.41-2.32)Si	98% pearlite + 2% martensite
Fe-3.2C-1.0Cu-0.32Mo-1.02Mn-(1.41-2.32)Si	(5.7-21.1)% austenite + (13-68)% ausferrite + (78-9)% pearlite + (3.1-1.5)% martensite
Fe-3.2C-1.0Cu-0.32Mo-1.21Mn-(1.41-2.32)Si	(10.2-23)% austenite + (23-70)% ausferrite + (61-1.7)% pearlite + (4.2-5.5)% martensite
Fe-3.2C-1.0Cu-0.32Mo-1.52Mn-(1.41-2.32)Si	(17-9.4)% austenite + (17-9.5)% ausferrite + (50.2-57.2)% pearlite + (4.2-5.5)% martensite
Fe-3.2C-1.0Cu-0.32Mo-2.34Mn-(2.10-2.32)Si	(6.7-7.4)% austenite + (93.3-92.6)% martensite

Pouring conditions: All the alloys were melted in induction furnace and poured at 1380-1420 °C into a resin bonded sand mold of 30 mm diameter
Influences of microstructure on mechanical properties in above alloys:
1. Pearlite + flake graphite give ultimate tensile strength (UTS) = 335 MPa; transverse fracture stress (TFS) = 560 MPa
2. Ausferrite + pearlite + graphite microstructures show that UTS and TFS increase with increasing ausferrite fraction. High Mn levels (>1.0%) promote the formation of carbides and martensite (up to 100% M)
3. Ausferrite + graphite show UTS up to 530 MPa and TFS up to 930 MPa. High Mo levels (0.9% N) promote the formation of carbides

The present work aims to understand the structure and properties of directly cast alloyed gray iron with ausferritic microstructure in comparison with austempered unalloyed and Ni alloyed gray iron.

2. Experimental Details

2.1 Melting Process for Austempered Gray Iron

A cast iron used for a certain vehicle application with composition (in wt.%) 3.4C-1.75Si-0.1S-0.04P-0.74Mn-0.36Cr-0.41Cu was used for austempering trials (Alloy 1). The component is a plate of diameter 381 mm and thickness 24.8 mm which was made in a sand casting mould from a 150 kg capacity induction furnace. The melt was poured with a 30 kg ladle. The iron was tapped at 1490 °C into a ladle and poured into the mould at 1400 °C along with inoculation of 0.2% ferrosilicon (70% Si) before casting.

A laboratory scale air induction melting was carried out to make Alloy 2 at 5 kg batch size, using a part of the plate sample along with other alloying additives in a 15 kW inductotherm furnace. Initially, the cut cast iron charge was melted, and to the molten metal Ni, Cu, ferro manganese (6.8C-70Mn), ferro-molybdenum (62%Mo-0.1%C) were added. Finally, misch metal (53Ce-24La-16Nd-5.78%-other rare earth-0.45Fe) of 0.5% was added along with 0.2% ferrosilicon (3%C-76%C) and the alloy was cast to a bar by pouring at a temperature of 1400 °C, directly into a sand mould of dimension 40 × 40 × 200 mm.

Cut samples from Alloys 1 and 2 were subjected to austempering treatment in a salt bath furnace as per details shown in Table 2.

2.2 Melting Process for Making Direct As-Cast Ausferritic Gray Iron

A gray iron of a target composition was melted in an Ashok Leyland vendor's foundry by modification of a Ni containing base pearlitic gray iron alloy melted in a 150 kg induction furnace. After casting the Ni containing cast iron for a certain component, a 30 kg leftover melt was modified with further addition of Ni, Cu, ferro manganese and ferro molybdenum to achieve a composition close to the final composition. The composition was checked by an online spectrometer analysis. The alloy was treated finally with misch metal in the final stages before pouring to a ladle at a temperature of 1480 °C. Just before casting the molten metal into the mould at about 1380 °C, powdered 0.2% of ferrosilicon [76%Si-1.2C] inoculant was added to the melt. The mould is a split sand mould made to form a rod of 30 mm diameter and 300 mm length. The final chemical analysis was carried out on the solidified casting. The composition was found to be 3.44C-2.02Si-0.64Ni-0.35Mo-1.21Mn-1.49Cu-0.37Cr-0.032Ce-0.07P-0.12S.

Table 2 Details of austempering treatment on the gray iron

Furnace	Modified set-up at IIT Madras
Sample dimensions	Samples: 20 × 20 × 150 mm (later machined to tensile samples according to ASTM E8)
Austenizing condition	900 °C for 90 min
Austempering condition	360 °C for 180 min
Austempering salt bath	7%$NaNO_3$-40%$NaNO_2$-53%KNO_3

2.3 Characterization Studies on the Alloys

The samples were examined for their chemistry using spectrographic technique. The phase analysis was carried out using XRD powder pattern on the samples using Fe K_α radiation (λ = 1.937 Å). The characterization of austenite and ferrite was done through XRD. The volume percent of austenite and ferrite was calculated according to ASTM E975. Microstructure evaluations were carried out in the as-cast samples cut from the ingot. Unetched microstructure was used to evaluate the graphite flake morphology, size and density distribution.

Etched microstructures were obtained with 2% Nital. Image analyzer was used to obtain the various phase constitutions. Hardness was measured with macro Vickers instrument at 5 kg load. An average of three values was reported for each alloy. Tensile specimens were prepared from the cast test bars according to ASTM E8 standards. Tensile testing was performed in DARTEC 200 kN UTM. Three specimens were tested for each data. Wear study was done according to the condition given in Table 3 at IIT Madras.

3. Results and Discussion

3.1 Chemistry of the Conventional Austempered and Direct As-Cast Ausferritic Alloy

The chemical compositions of the alloys chosen for the study are shown in Table 4. Xu et al. (Ref 1) have studied as-cast ausferritic irons development with various compositions. One of their hypoeutectic iron composition (in wt.%) 3.2C-1.0Cu-0.32Mo-1.52Mn-2.1Si in the as-cast condition showed a mixed microstructure consisting of ~34% martensite and ~9% austenite in addition to ausferritic structure with strength of 350 MPa. This composition, taken as a basis, was altered by alloying modification to achieve a completely ausferritic microstructure in the as-cast condition. Such direct as-cast ausferritic alloys can avoid salt bath heat treatment required. The alloy modification carried out involved addition of Ni. This alloy made was also compared with two conventionally austempered gray irons one with and other without Ni additions. In the present study, the conventionally austempered gray irons chosen are Alloys 1 and 2 while the direct as-cast ausferritic iron is Alloy 3. The compositions are shown in Table 4. The compositions show that in Alloy 1, the major alloying elements are 0.74Mn-0.36Cr-0.41Cu and in Alloy 2 it is 0.7Mn-0.5Cu-0.37Mo-0.62Ni-0.003Ce. Both these irons in the as-cast condition showed pearlitic gray iron microstructure. The direct as-cast ausferritic alloy iron casting had a composition 0.64Ni-0.35Mo-1.21Mn-1.49Cu-0.37Cr-0.003Ce.

Among the alloying additives in these two irons, it is well known that Mn, Mo, Cr and V segregate to eutectic boundaries. In Alloy 1, the 0.74%Mn-0.36%Cr is there while in Alloy 2 0.7Mn-0.7Cr-0.37Mo is expected to give higher segregation. The direct as-cast ausferritic Alloy 3 has much larger concentration of segregation prone alloying elements 0.35Mo-1.21Mn-1.49Cu-0.37Cr. The potency of segregating elements is reported by Mulins (Ref 8), which shows that segregation tendency follows the order Mo > Cr > Mn. In the present series of alloys, Cr is an unintentional alloying additive that has come during melting the scrap iron used. It can be assessed that segregation of elements to eutectic cell boundaries will be of the order Alloy 3 > Alloy 2 > Alloy 1.

The elements that are added in austempered irons to achieve higher hardenability or uniformity in ausferritic structure are Ni, Mo and Cu. It can be assessed that Alloy 1 has only 0.41 Cu while Alloy 2 has 0.5Cu-0.62Ni-0.37Mo and Alloy 3 has 0.64Ni-1.49Cu-0.35Mo. It can be assessed that hardenability follows the order as Alloy 3 > Alloy 2 > Alloy 1.

The role of the alloying elements in the present series of alloys may then be considered. Nickel is a graphite former and pearlite stabilizer in a gray iron. However, it is stated that Ni does not stabilize the pearlite, but breaks down the pearlite apart from improving the ausferrite through hardenability.

Table 3 Experimental conditions for wear testing

Test facility	Pin-on-disc test rig
Wear test standard	ASTM G99-05
Wear pin dimension	9 mm diameter × 15 mm length
Wear disc	Through-thickness hardened steel: 752 VHN (62 HR_c); composition (%): 1.08C-1.34Cr-0.4Mn-0.38Si-0.026P-0.046S
Normal load	170 N
Sliding velocity	0.4 m/s ($P \times V = 1.07$)
Sliding distances used	1000, 1500 and 2000 m

Table 4 Comparison of direct ausferrite structure obtained with close by composition suggested by Xu et al. (Ref 1)

Features/properties	Alloy 1	Alloy 2	Alloy 3	Xu et al. (Ref 1)
Composition, wt.%	3.4C-1.75Si-0.1S-0.038P-0.74Mn-.36Cr-0.41Cu	3.9C-1.92Si-0.62Ni-0.37Mo-0.7Mn-0.5Cu-0.7Cr-0.003Ce-0.06S-0.032P	3.44C-2.02Si-0.64Ni-0.35Mo-1.21Mn-1.49Cu-0.37Cr-0.003Ce-0.07P-0.12S	3.2C-2.1Si-0.32Mo-1.52Mn-1.0Cu
Conditions	Austempered at 360 °C	Austempered at 360 °C	As-cast direct ausferrite	As-cast
CE, wt.%	3.88	4.42	4.00	3.64
Eutectic cell size, μm	877	900	789	…
Graphite flake type (a)	4D	4C	5D	…
Graphite flake size, μm	359	465	350	…
Mean flake size, μm	28.5	41	23	…
Graphite flakes area, %	11.0	20.8	9.3	…
Graphite flakes, mm^2	724	312	864	…
Carbide volume, %	0.7	0.8	1.5	…
Austenite volume (from XRD), %	15.98	25.75	34.61	
Austenite lattice parameter, Å	3.6128	3.6068	3.6068	…
Ferrite volume (from XRD), %	72.22	54.25	30.75	…
Ferrite cell size (from XRD), μm	0.239	0.076	0.15	…
Ferrite lattice parameter, Å	2.8689	2.8689	2.8643	…

(a) Measured as per ASTM A247
CE = %C + 0.23 (%Si) – 0.03 (%Mn) + 0.32 (%P) + 0.64 (%S) + 0.02 (%Ni) + 0.06 (%Cr) (Ref 13)

In other words, Ni containing ausferritic structures may be expected to have more uniform ausferritic microstructures. Manganese is a pearlite stabilizer in gray iron but a good promoter of hardenability in ausferritic irons, although it segregates to eutectic boundaries. Copper is a pearlite promoter in gray iron; however, it improves hardenability moderately as ausferritic irons. Molybdenum is another element which promotes and stabilizes pearlite in gray iron but enhances hardenability in ausferritic iron. However, it has very high segregation tendencies. The metalloid elements Sb is a pearlite former, while As and Sn are potent pearlite former and stabilizers in gray irons. They modify the graphite shapes.

Rare earth Ce addition also alters the graphite shape. It has been reported that Ce in gray iron refines the structure by thinning the graphite flakes (Ref 9). Ce has a tendency to react with sulphur as well and can desulphurize the bath. Although 0.1% Ce was added to the molten metal bath, in the present study Ce recovery was just 0.003%.

In the present study, Alloy 3 is a Ni and Cu modified alloy of Xu et al. (Ref 1). Compared to their alloy, Alloy 3 had 0.64% Ni with excess addition 0.49% Cu. The Mn content was lower by 0.31%. Though not an intentional alloying additive, the carbon content was also more by 0.24%. The modified alloy in the present study showed fully uniform ausferritic structure without martensite. Hence, the alloying elements have had a role in suppressing martensite and promoting ausferritic structure. In austempered alloys, there is the carbon stabilized austenite phase and in those micro volumes of austenite, elements such as Ni, Cu and C may be expected to serve the role of stabilizing the austenite. Hence, even though in conventional gray iron Ni may not have any role in stabilizing austenite, the austenite in ADI can have enhanced austenite stabilizing tendency when alloyed with elements Ni, Cu and carbon.

The microstructure and properties of the direct as-cast ausferritic composition (Alloy 3) was compared with two conventionally austempered gray irons austempered at 360 °C. This austempering condition was chosen as the microstructure had well resolved ausferritic microstructure free of martensite for comparison with the direct ausferritic alloys.

3.2 Microstructure and Phase Analysis

The XRD powder pattern analysis of the alloys studied in Fig. 1 shows that the unalloyed austempered hypoeutectic cast iron Alloy 1 shows very sharp high intensity austenite and ferrite diffraction peaks. Alloys 1 and 2 show peaks at identical 2θ values although the peaks differ in intensities. The $(111)_\gamma$ peak is not resolved in Alloy 1. The direct ausferritic alloy (Alloy 3) follows the diffraction pattern exactly matching that of the alloyed hypereutectic austempered gray iron (Alloy 2) with a clear resolution of $(111)_\gamma$ peak. The x-ray diffraction does not reveal the significant presence of any other major phases.

The typical microstructures obtained in the alloys are as shown in Fig. 2(a) and (b). The microstructural features of the alloys studied are compiled in Table 4. An assessment was made on the equilibrium solidification of the alloys studied. The various phases formed as per equilibrium solidification till the complete solid state achievement are shown in Table 5. The equilibrium flake volume percentage as per equilibrium solidification is found to be almost matching with the hypoeutectic alloys 1 and 2. In the case of Alloy 3, the measured carbon volume fraction was 20.8% while the total volume percent is much lower.

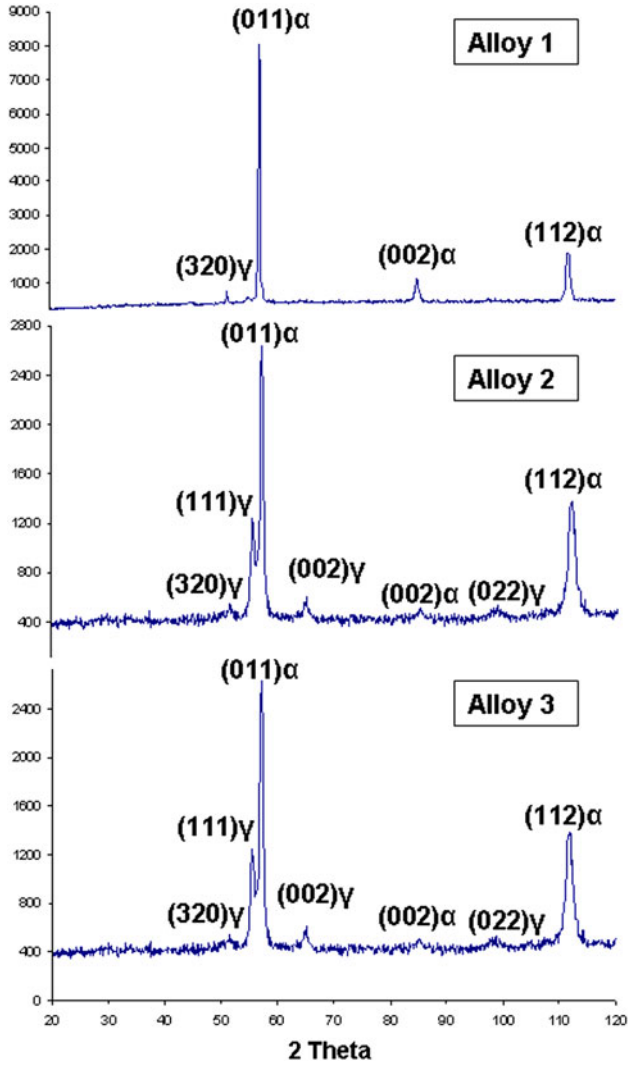

Fig. 1 XRD phase analysis showing complete ausferrite microstructure in the alloys studied. Sharp high-intensity peaks are observed in the unalloyed austempered alloys. The austempered and direct as-cast ausferritic alloys show completely matching peaks

The unetched microstructures (Fig. 2a) obtained show that the hypoeutectic alloys (Alloys 1 and 3), in general, showed dendritic morphology with graphite distribution in the interdendritic regions. The flake morphology was appearing in between that of Type D and Type E. In some regions, islands of graphite conforming to Type D were observed while in some other regions long primary dendritic structures could be observed. The hypoeutectic alloys initially form austenite dendrite during solidification and the solute-rich interdendritic liquid nucleates graphite in the interdendritic regions. One reason for the formation of Type D or Type E could be due to high super heat at pouring temperature which is reported to promote higher under cooling during solidification. The graphite area fraction of Alloy 1 is 11% and that of Alloy 3 is 9.3%. The presence of higher carbide forming elements could have reduced the higher graphite formation in Alloy 3. The hypereutectic alloy (Alloy 2) showed Type C graphite, as primary graphite during solidification forms thicker primary graphite followed by eutectic solidification where thinner graphite flake is seen. In Alloy 2, the presence of primary graphite and in addition the inoculant seemed to have lowered

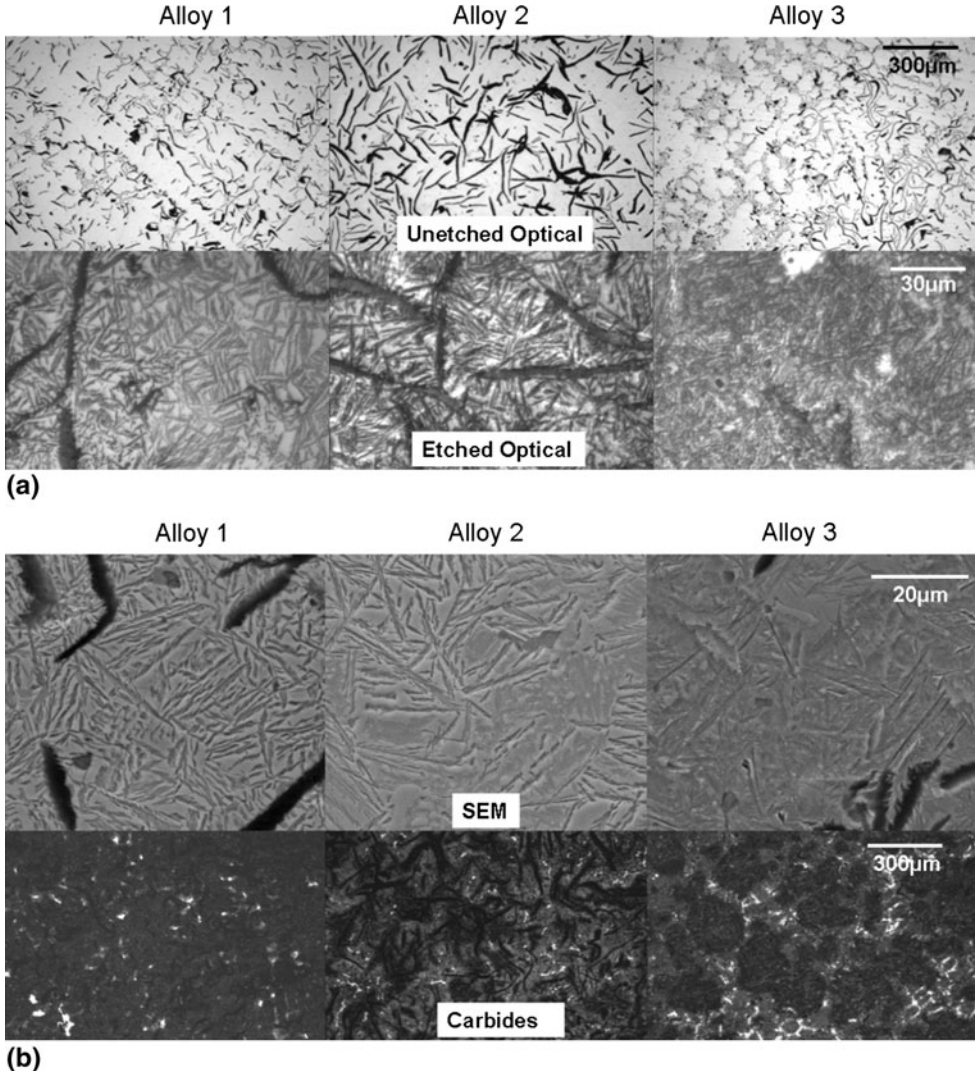

Fig. 2 (a) Optical micrographs of unetched alloys showing graphite morphology and etched alloys showing ausferritic structure. (b) SEM micrographs of alloys showing ausferritic structure and the distribution of carbides in the eutectic cell boundaries for the various alloys

Table 5 Equilibrium solidification from the phase diagram to assess the extent of graphite flake and austenite phase formed in the alloys

Features/properties	Alloy 1	Alloy 2	Alloy 3	Xu et al. (Ref 1)
Carbon equivalent, wt.%	3.88	4.42	4.00	3.64
Class	Hypo	Hyper	Hypo	Hypo
Equilibrium phases formed compared with actual				
Eutectic carbon, wt.%	3.75	3.70	3.66	3.64
Primary austenite, %	16.38	…	10.83	21.45
Primary graphite, %	…	0.21	…	…
Eutectic austenite fraction	0.84	0.98	0.89	0.79
Eutectic graphite fraction	0.02	0.02	0.02	0.02
Eutectic austenite, %	69.93	97.66	79.52	61.70
Eutectic graphite, %	1.83	2.13	1.87	1.63
Total % austenite in the matrix	86.31	97.66	90.35	83.15
Total % graphite in the matrix	1.83	2.34	1.87	1.63
Vol.% of graphite	7.38	8.27	7.22	6.85
Measured vol.% graphite	11.0	20.8	9.3	~8
Vol.% of austenite	92.62	91.73	92.78	93.15

the under cooling, leading to extensive graphite flake distribution in the matrix.

The etched microstructures of all the alloys show ferrite needles in austenite (Fig. 2a). This is seen in the austempered alloys as well as the direct as-cast alloys. The direct cast ausferritic alloy (Alloy 3) shows much finer ferrite needles in austenite in optical micrograph (1000×). The alloys austempered at 360 °C show an austenite content of 16-25% and ferrite content of 54-72% (Table 4 and Fig. 2). The direct ausferrite alloys show lower ferrite content of 31% and austenite of 35%. In other words, the structure obtained may be equivalent to lower austempering temperatures of the order say 320 °C. The corresponding SEM micrographs are as shown in Fig. 2(b) with ausferritic structure.

Debey Scherer formula was used to calculate the mean sizes of ferrite laths (Ref 10):

$$d = 0.9\lambda/\beta \cos(\theta) \qquad \text{(Eq 1)}$$

where λ is the wave length of incident x-ray, β the breadth of the $(211)_\alpha$ peak at half intensity height in radians, and θ is the Bragg angle.

The conventionally austempered iron Alloy 1 without other alloying elements shows average ferrite lath sizes of 0.239 μm. The conventionally austempered Ni and Mo alloyed austempered cast iron (Alloy 2) shows much finer lath sizes of 0.076 μm. The direct ausferritic as-cast alloy (Alloy 3) shows 0.15 μm. While the lattice parameter of ferrite is almost same in all the alloys due to limited solubility of C in ferrite, the carbon content of austenite in the Alloy 1 is higher at 3.6128 Å. The alloyed austempered gray iron and direct ausferrite alloy show same lattice parameter values.

The carbide distribution is another aspect to be examined in the alloys studied. The carbides are found distributed at the eutectic cell boundaries as shown in Fig. 2(b). Alloy 1 has lowest carbide content of 0.7%, which may be due to lower content of carbide forming elements. The Alloy 2 has still higher contents of carbide formers and accordingly its carbide volume fraction was 0.8%. Alloy 3 with the highest carbide forming elements had a carbide content 1.5%. It is well known that Mo and Cr can segregate toward eutectic cell boundary to form hard wear-resistant carbides (Ref 1, 11). Even Cu in excess of 0.6-0.7% can cause segregation (Ref 12).

3.3 Mechanical Properties

The mechanical and wear properties of the alloys are shown in Table 6 and Fig. 3. The alloyed austempered gray iron Alloy 1 shows lowest strength of 235 MPa and the corresponding microstructure shows evenly distributed ferrite laths in austenite (Table 6). The austempered hypoeutectic Alloy 1 showed a marginally higher strength level to that of the Alloy 3 at about 250 MPa. The corresponding microstructure is similar to that of the Alloy 2. The direct ausferrite alloy (Alloy 3) shows a strength level of 392 MPa, which is more than 60% of the lowest strength. The higher strength may be attributed to higher volume fraction (35%) of stronger austenite than the austempered alloys (16-26%). In addition, there is significant presence of carbide observed in the direct as-cast alloy which may have contributed to such a higher strength.

The austempering of the alloys in the present study was done at a temperature of 360 °C, where the austempering reaction is complete, and hence show lower strengths. The direct ausferritic alloy has not undergone any controlled tempering. The ausferrite has formed due to the shift if the C-curve associated with the increase in alloying elemental contents. Hence, although the type of phases obtained in the direct ausferrite alloy is same as that of the other two alloys, the morphology and distribution of ferrite in austenite appear to be different. It can be seen that the direct ausferritic alloy has a microstructure that has finer randomly oriented ferrite in austenite. The laths were resolvable only at higher magnification. There was also no clear evidence for the presence of martensite in the microstructure. The alloy studied by Xu et al. (Ref 1) showed strength of 350 MPa and its microstructure had significant quantity of martensite. The present alloy, on the other hand, shows very high strengths associated with the ferrite lath distribution and solid solution strengthening of the alloying elements in the austenite phase.

The fractographic features of the mechanically failed sample were analyzed only in the direct ausferritic alloy (Alloy 3). The fractured surface showed mixed mode failure where weak fractured zones are observed along the graphite flakes as shown in Fig. 4(a)-(c). In certain regions, dimple facets were seen as shown in Fig. 4(c). Hence, the presence of ductile region at high strength is another aspect that improves toughness. The crack propagation has been delayed by these dimples and hence the toughness also would have improved.

3.4 Wear Properties

The specific wear rate and coefficient of friction of alloys are compared in Fig. 5. The ausferritic structure in general improves wear and abrasion resistance, as the austenite at the

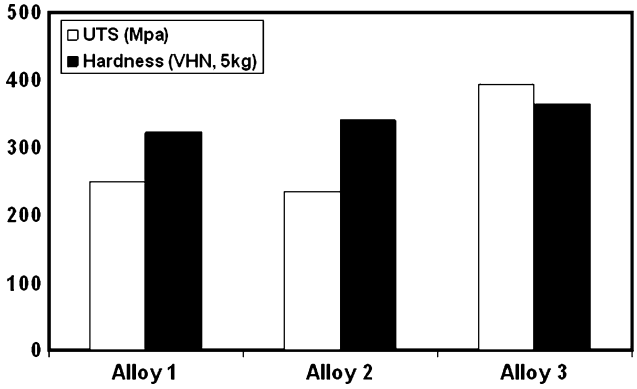

Fig. 3 Mechanical properties of the austempered alloys compared with direct ausferritic alloys

Table 6 Mechanical properties of the austempered and direct cast ausferritic alloys

Alloy	Composition, wt.%	CE, wt.%	Phases	Hardness, VHN_{5kg}	UTS, MPa	Specific wear rate ($\times 10^{-7}$), g/Nm	Friction coefficient
Xu et al. (Ref 1, 2)	3.2C-2.1Si-1.0Cu-0.32Mo-1.52Mn	3.64	9.4% austenite + 56.4% ausferrite + 34.2% martensite	…	350	…	…
Alloy 1	3.4C-1.75Si-0.1S-0.038P-0.74Mn-0.36Cr-0.41Cu	3.88	100% ausferrite	323	250	2.6	0.39
Alloy 2	[3.9C-1.92Si-0.62Ni-0.37Mo]-0.7Mn-0.7Cr-0.5Cu-0.003Ce-0.06S-0.032P	4.42	100% ausferrite	341	235	0.6	0.37
Alloy 3	[3.44C-2.02Si-0.64Ni-0.35Mo]-1.21Mn-0.37Cr-1.49Cu-0.03Ce-0.12S-0.07P	4.00	100% ausferrite	363	392	0.68	0.30

CE = %C + 0.23 (%Si) − 0.03 (%Mn) + 0.32 (%P) + 0.64 (%S) + 0.02 (%Ni) + 0.06 (%Cr) (Ref 13)

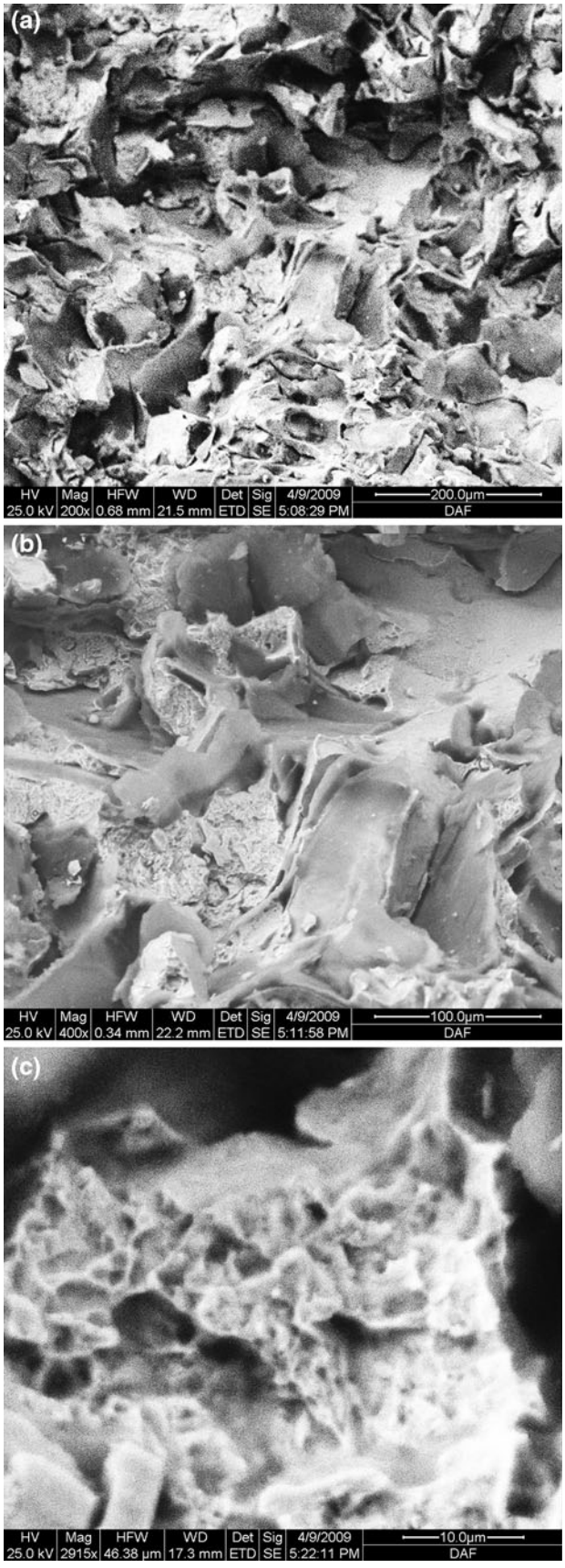

Fig. 4 (a-c) Fractograph of the as-cast ausferritic structure showing brittle transgranular failure along plate-like graphite flakes along with zones of dimples (~25%)

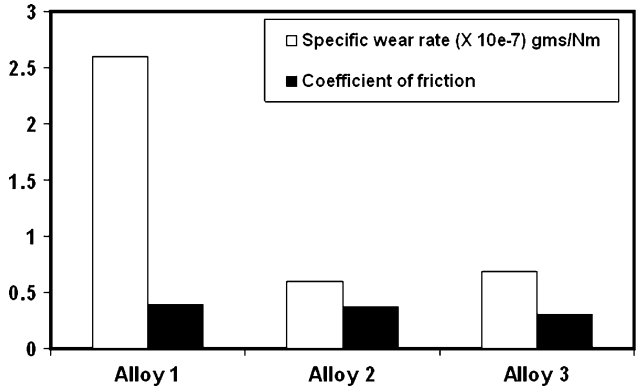

Fig. 5 The wear and friction properties of the austempered alloys compared with direct ausferritic alloy

rubbing interface transforms to strain-induced martensite (Ref 5). This resists further deformation of the surface. Alloys 2 and 3 in the present study show very low wear rate compared to Alloy 1. The wear rate of Alloys 2 and 3 were four to five times lower than Alloy 1. The lowest wear rate was, however, found in the austempered alloyed gray iron (Alloy 2). Marginally higher wear rate was observed in the direct ausferritic alloy (Alloy 3) as well.

The coefficients of friction of all the alloys are below 0.4. The squeaking sound, which is a typical characteristic of adhesive wear process during sliding, was significantly less. The graphite flake releases carbon into the interface during sliding and reduced wear and friction considerably. The improvement in wear properties due to ausferritic matrix along with graphite flakes has been reported in literatures (Ref 14-16). The wear debris generated is a fine mixture of graphite and iron oxide particulates. Hence, it is clear that direct ausferritic alloy shows wear properties equal to alloyed austempered irons.

4. Conclusions

A direct as-cast ausferritic gray iron could be obtained in a composition 3.44C-2.02Si-0.64Ni-0.35Mo-1.21Mn-0.37Cr-1.49Cu-0.003Ce-0.12S-0.07P without the presence of martensite. There was no detectable presence of martensite from the presence of Ni and Mo along with high carbon in Alloys 2 and 3. The graphite flakes formed are higher and much finer than the other alloys which have influenced tensile strength, wear resistance and coefficient of friction. This composition shows wear resistance comparable to austempered alloyed gray iron. The wear resistance was four times better than austempered Alloy 1. But the wear rate of direct as-cast ausferritic alloy was similar to austempered Ni and Mo alloyed gray iron, indicating that the studied composition can be equally wear resistant without additional austempering process.

Acknowledgments

The authors thank Mr. B. S. Sharath of Technorings, Shimoga, for providing the direct ausferritic alloy. The authors also gratefully acknowledge Mr. B. Gopalakrishna, D. Venkateshwara Rao and Mr. Prabhakara Rao of Defense Metallurgical and Research Laboratory, Hyderabad, for their assistance in obtaining the required alloys.

References

1. W. Xu, M. Ferry, and Y. Wang, Influence of Alloying Elements on As-Cast Microstructure and Strength of Gray Iron, *Mater. Sci. Eng. A*, 2005, **390**, p 326–333
2. M. Ferry and W. Xu, Microstructural and Crystallographic Features of Ausferrite in As-Cast Gray Iron, *Mater. Charact.*, 2004, **53**, p 43–49
3. G. Cueva, A. Sinatora, W.L. Guesser, and A.P. Tschiptschin, Wear Resistance of Cast Irons Used in Brake Disc Rotors, *Wear*, 2003, **255**(7–12), p 1256–1260
4. J. Porkert and W. Lotz, Optimized Gray Cast Iron Plate Alloy for Utility Brake Disc, U.S. Patent 5,894,010, 1999
5. R. Ritha Kumari and P. Prasad Rao, Study of Wear Behaviour of Austempered Ductile Iron, *J. Mater. Sci.*, 2009, **44**, p 1082–1093
6. T.J. Bedwell and J.F. Miller, Austempered Gray Iron Cylinder Liner and Method of Manufacture, U.S. Patent 6,732,698 B1, 2004
7. K.B. Rundman, J.R. Parolini, and D.J. Moore, Relationship Between Tensile Properties and Matrix Microstructure in Austempered Gray Iron AFS Transactions Paper, 05-145(05), 2005, p 1–15
8. J.D. Mulins, Element Segregation Factor, *Sorel Met. Rev.*, 2006, p 85
9. J. Yamabe, M. Takagi, T. Matsui, T. Kimura, and M. Sasaki, Development of Disc Brake Rotors for Trucks with High Thermal Fatigue Strength, *JSAE Rev.*, 2002, **23**, p 105–112
10. S.K. Putatunda, Development of Austempered Ductile Cast Iron (ADI) with Simultaneous High Yield Strength and Fracture Toughness by a Novel Two-Step Austempering Process, *Mater. Sci. Eng. A*, 2001, **315**, p 70–80
11. G.S. Cho, K.H. Choe, K.W. Lee, and A. Ikenaga, Effects of Alloying Elements on the Microstructures and Mechanical Properties of Heavy Section Ductile Cast Iron, *J. Mater. Sci. Technol.*, 2007, **23**(1), p 97–101
12. V.P. Polovinchuk and A.A. Zhukov, Copper in Low-Alloy Sulphur Cast Iron, *Metallovedenie i Termicheskaya Obrabotka Metallov*, 1992, **5**, p 43–44
13. T. Kanno, I. Kang, T. Kikuchi, K. Hayashi, and Y. Maruyama, Relationship Between Primary Crystal Temperature and Carbon Equivalent in Cast Iron, *J. Mater. Sci. Technol.*, 2008, **24**(3), p 325–326
14. C.-H. Hsu, Y.-H. Shy, Y.-H. Yu, and S.-C. Lee, Effect of Austempering Heat Treatment on Fracture Toughness of Copper Alloyed Gray Iron, *Mater. Chem. Phys.*, 2000, **63**, p 75–81
15. A.R. Ghaderi, M. Nili Ahmadabadi, and H.M. Ghasemi, Effect of Graphite Morphologies on the Tribological Behavior of Austempered Cast Iron, *Wear*, 2003, **255**, p 410–416
16. S. Yazdani and M.A. Rahimi, Wear Behavior of an Austempered Ductile Iron Containing Mo-Ni-Cu, *Mater. Sci. Forum*, 2005, **475**, p 199–202